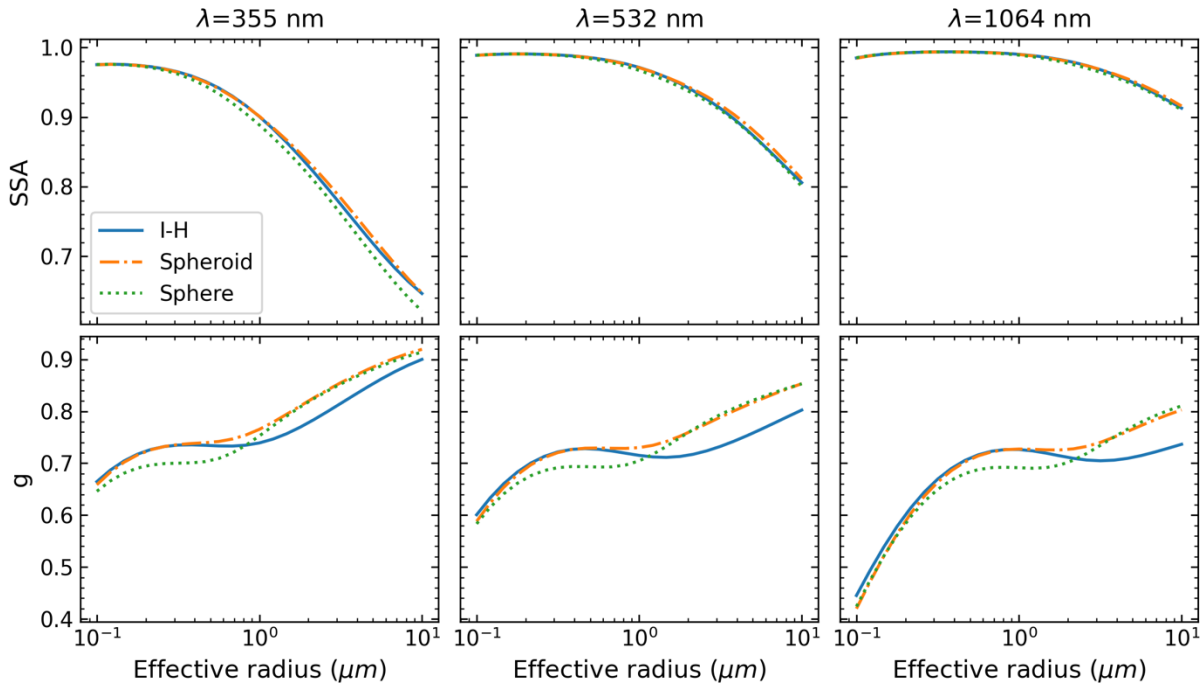

Figure 1. Single-Scattering albedo (SSA) and asymmetry factor (g) simulated with the Irregular-Hexahedral (I-H) model (Saito et al., 2021) (solid line), Spheroid model (Dubovik et al., 2006) (dash-dot line) and Sphere model (Dubovik et al., 2006) (dot line) against particle effective radius (r_{eff}) at 355, 532 and 1064 nm. The r_{eff} is calculated from a set of lognormal volume size distributions with a geometry standard deviation of 0.6 and the unit of volume concentration. The real part and imaginary part of refractive index is n = 1.5 and k = 0.004, respectively.

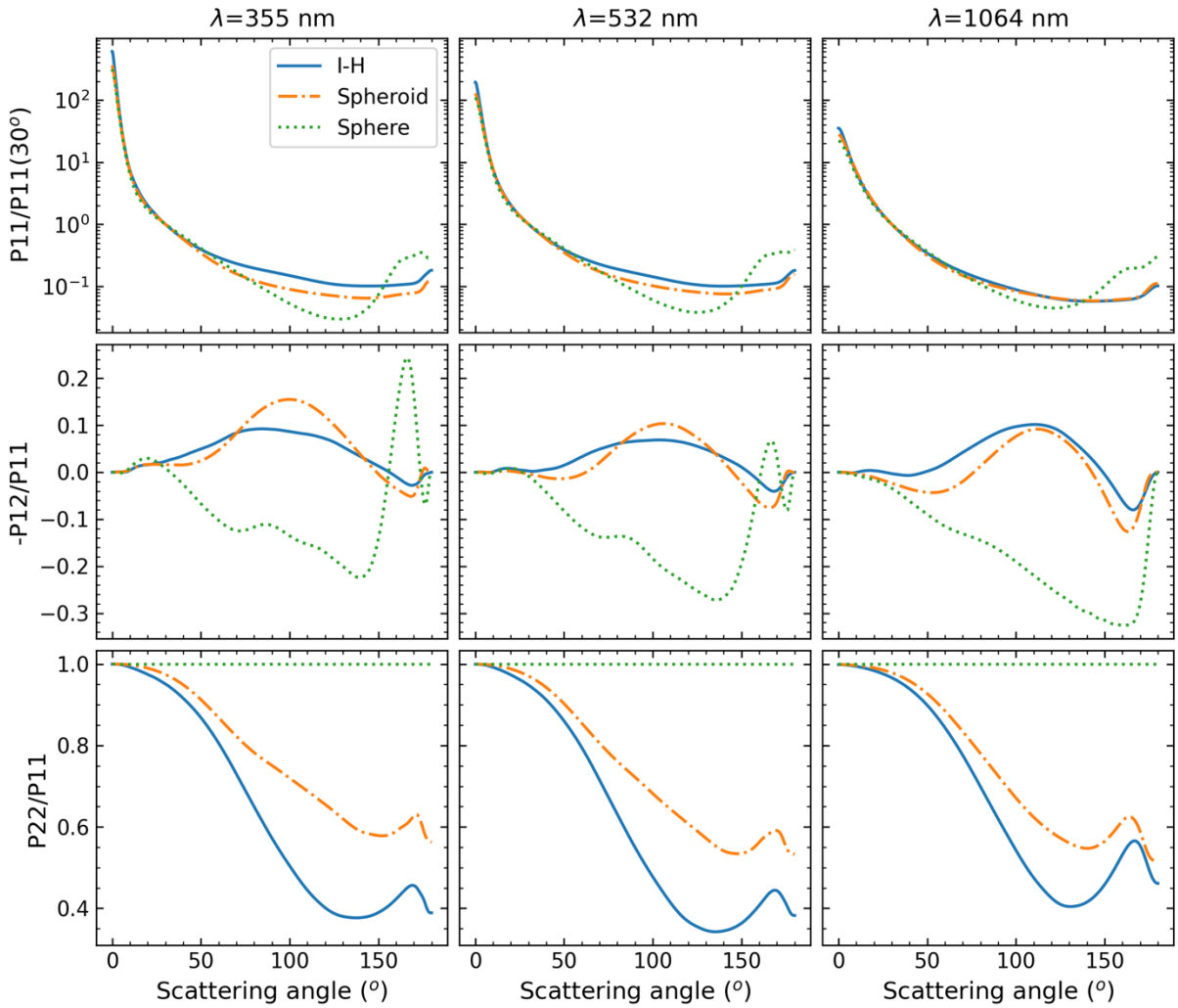

Figure 2. Same as Figure 1 but for the angular distribution of normalized phase matrix elements: P11 (normalized to P11 at 30°), -P12 (normalized to P11) and P22 (normalized to P11).

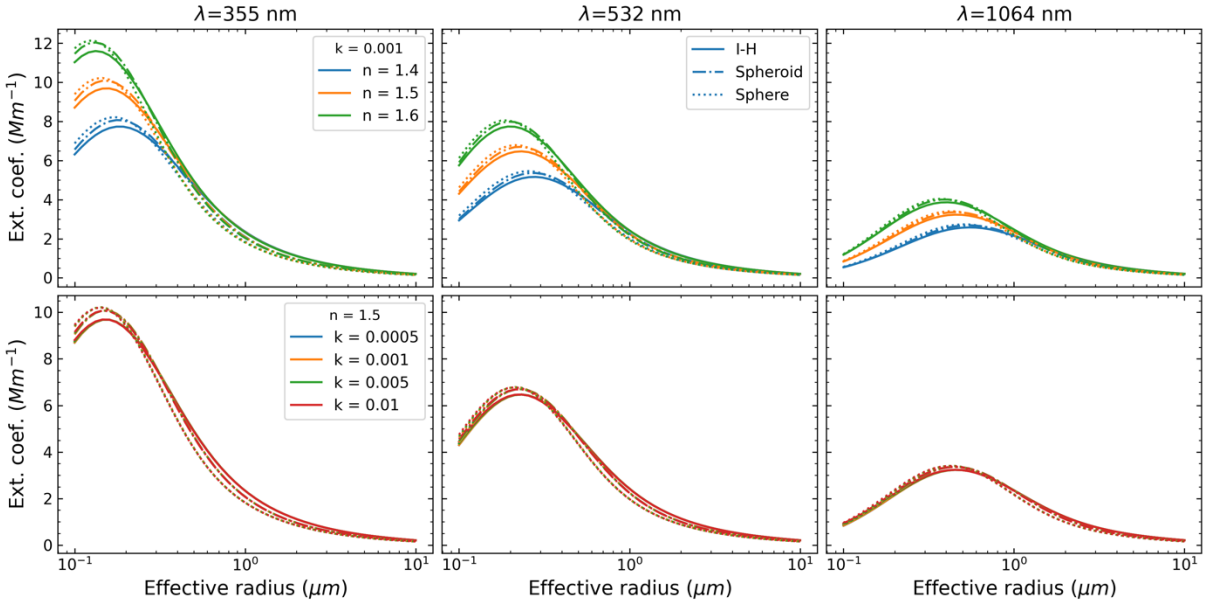

Figure 3. Extinction coefficient (α) simulated with the Irregular-Hexahedral (I-H) model (solid line), Spheroid model (dash-dot line) and Sphere model (dot line) against particle effective radius (r_{eff}) for different real parts

(*n,* the first row) and imaginary parts (*k,* the second row) of complex refractive index (CRI) at 355, 532 and 1064 nm. The r_{eff} is calculated in the same way with Figure 1.

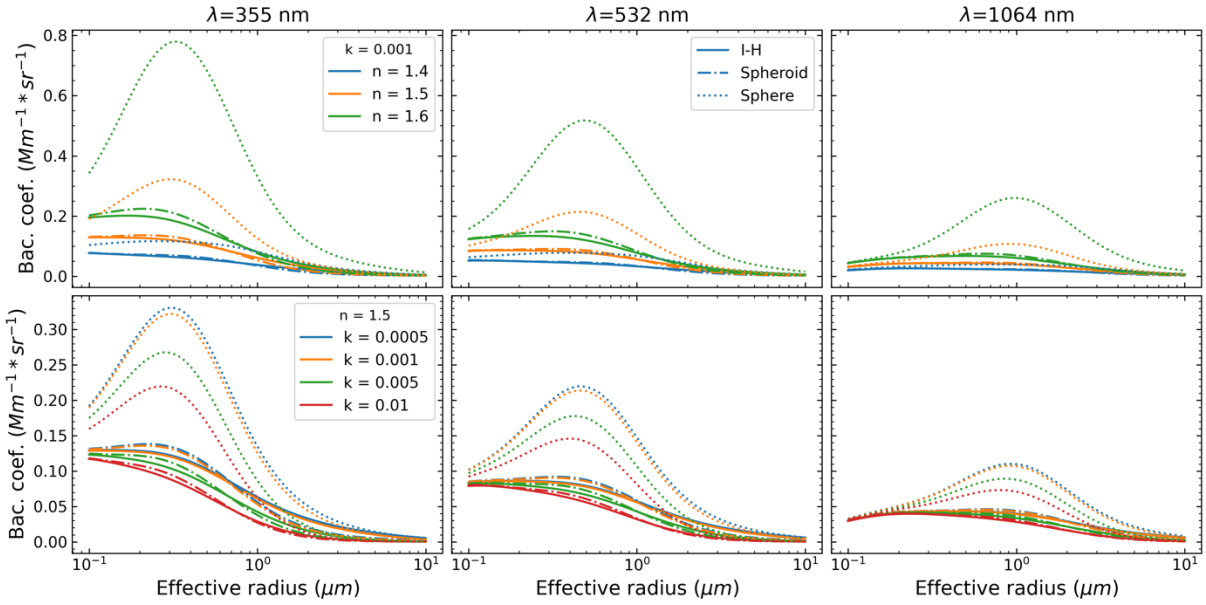

Figure 4. Same as Figure 3 but for the backscattering coefficient (β).

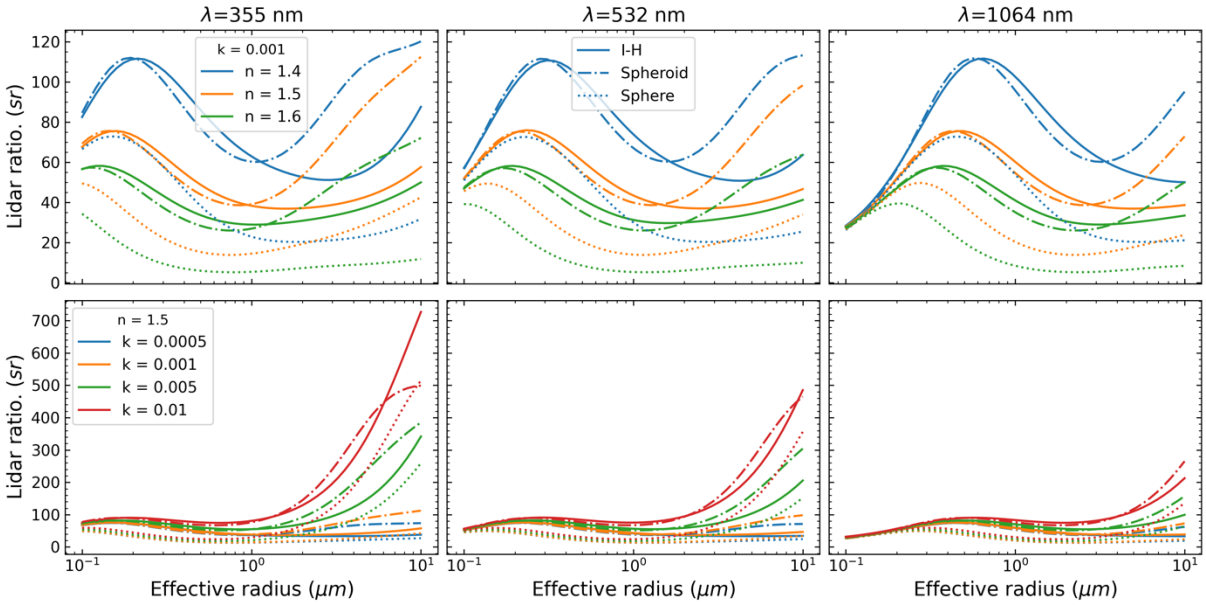

Figure 5. Same as Figure 3 but for the lidar ratio.

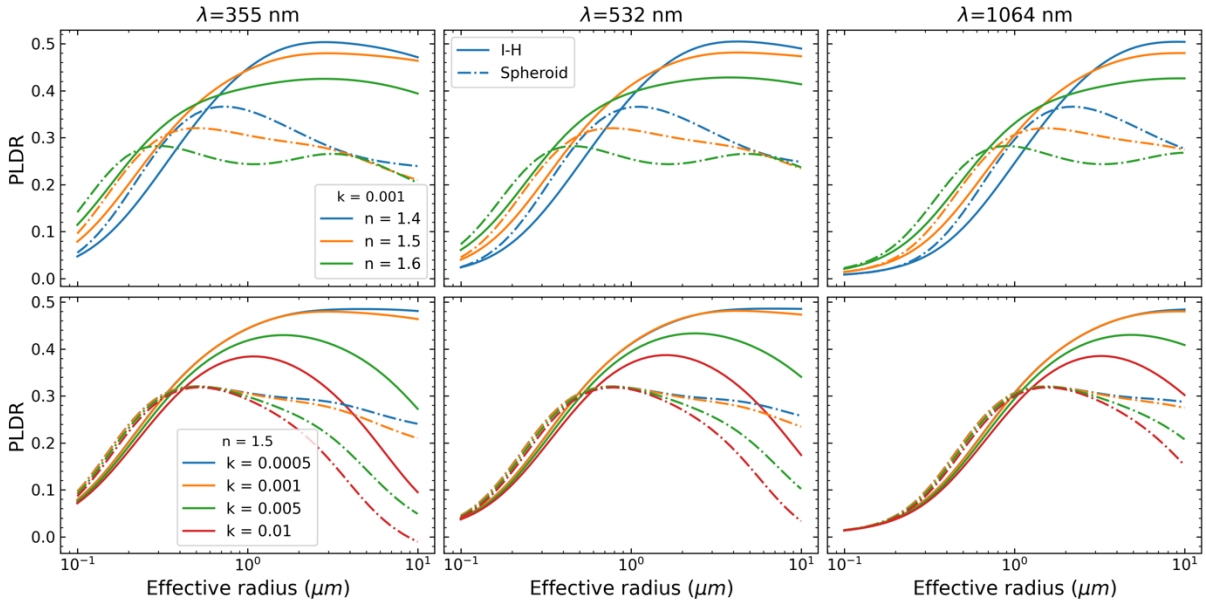

Figure 6. Same as Figure 3 but for the particle linear depolarization ratio (PLDR). Note the PLDR of spherical particles is always zero and not shown here.

Table 1. Parameterization of aerosol microphysical properties for generating synthetic measurements and retrieval simulation.

Volume size distribution (VSD) – lognormal distribution	$v(r) = \frac{dV}{dlnr} = \frac{1}{\sqrt{2\pi}S}\exp\left[-\frac{(lnr - lnr_v)^2}{2S^2}\right]$
r_V (μm)	1 (Transported dust), 2 (Fresh dust)
S	0.6
Real part of refractive index *(n)*	1.4, 1.5, 1.6
Imaginary part of refractive index *(k)*	0.001, 0.005, 0.009

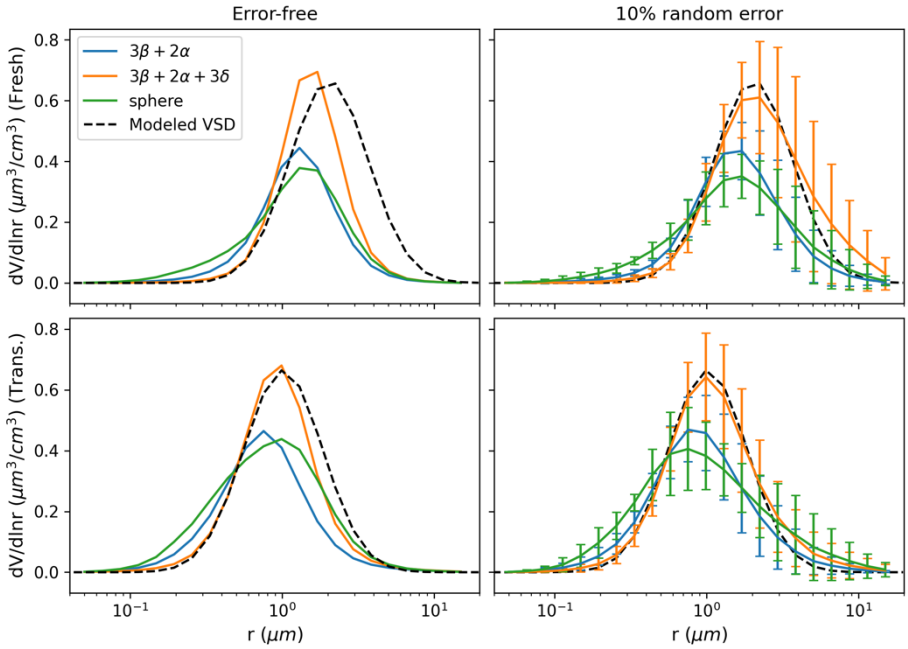

Figure 7. Volume size distribution (VSD) retrieved from synthetic 3β (backscattering coefficients at 355, 532 and 1064 nm) + 2α (extinction coefficients at 355, 532 nm) + 3δ (depolarization ratio at 355, 532 and 1064 nm) measurements. The synthetic measurements are calculated with the Irregular-Hexahedral (I-H) model from a modeled VSD (dashed line) representing the "fresh dust" (first row, having a larger mode radius) and the "transported dust" (second row, with a smaller mode radius) with n = 1.5 and k = 0.005 (see Table 1 for more details). The results are derived by using the I-H model to invert only the 3β + 2α data (blue), the full 3β + 2α +

3δ data (orange), as well as using the Sphere model to invert the 3β + 2α data (green). The left column corresponds to the results when the synthetic measurements are free from measurement uncertainty, while the right column corresponds to the synthetic measurements are perturbed by 10% measurement uncertainty. For the latter, the results are averages of 100 runs with error bars representing the statistical standard deviation.

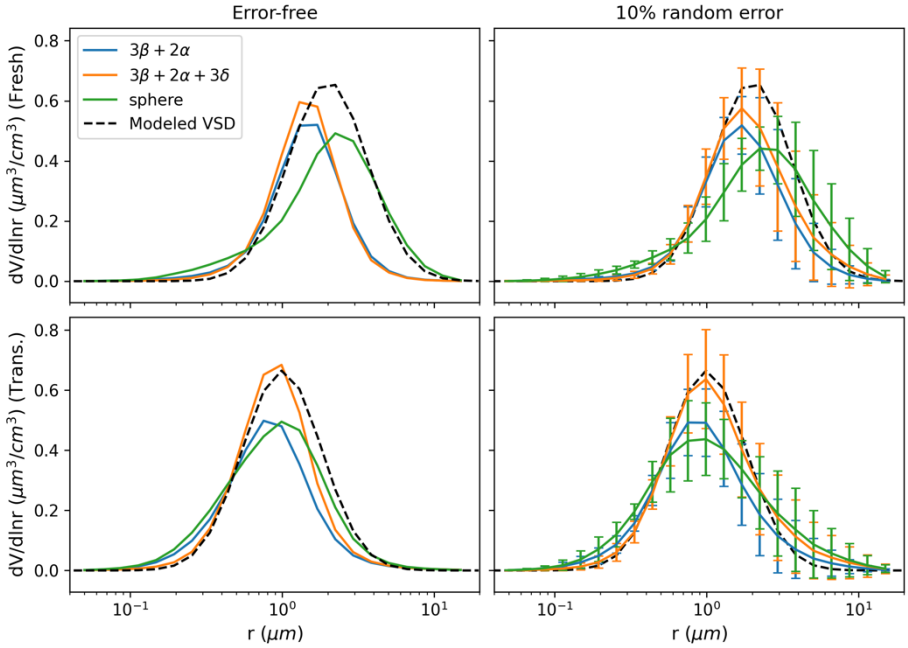

Figure 8. Same as Figure 7 but the synthetic measurements are calculated and inverted with the Spheroid model.

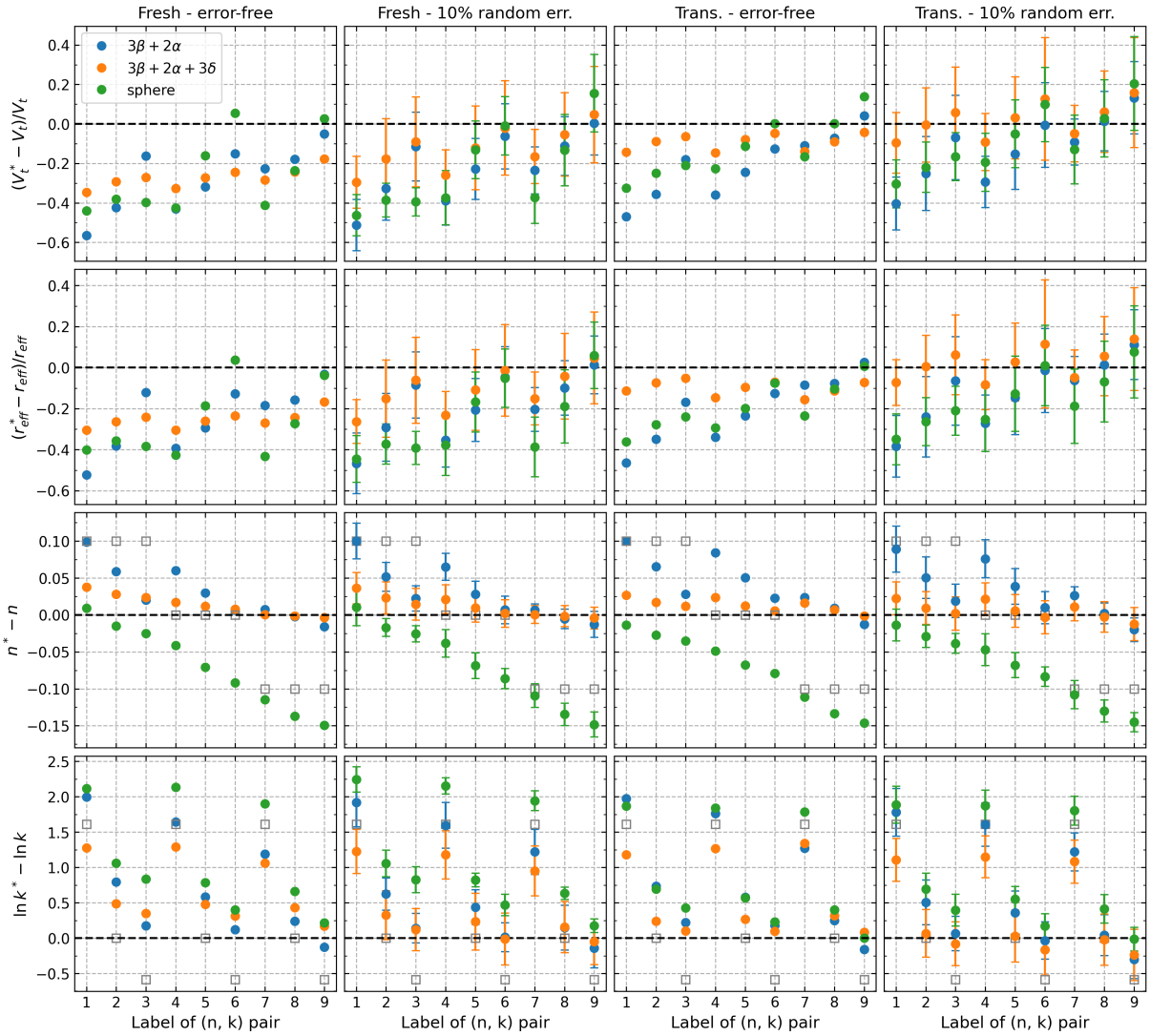

Figure 9. Differences between the retrieved values (with superscript *) and the modeled values for particle volume concentration (V_t), effective radius (r_{eff}), real part (n) and imaginary part (k). The retrieved values are derived by inverting synthetic measurements simulated with the Spheroid model and the modeled particle microphysical properties. Among them, the results by inverting 3β + 2α + 3δ and 3β + 2α with the Spheroid model are shown in orange and blue, respectively, while the results by inverting 3β + 2α with the Sphere model are shown in green. The results correspond to the modeled (n, k) whose label numbers are shown as the x-axis and can be checked from Table 2. For retrieving n and k, due to the algorithmic principle a priori assumption is needed and its difference from the modeled value is also shown as the hollow square (A complete description of the retrieval algorithm can be found in Chang et al., 2022). The columns show the results for different VSD types (see Table 1) and influence of measurement error. The way of studying the measurement error is the same as explained in Figure 7-8.

Table 2. Labels of the (n, k) pairs in Figure 9.

1	2	3	4	5	6	7	8	9
(1.4, 0.001)	(1.4, 0.005)	(1.4, 0.009)	(1.5, 0.001)	(1.5, 0.005)	(1.5, 0.009)	(1.6, 0.001)	(1.6, 0.005)	(1.6, 0.009)

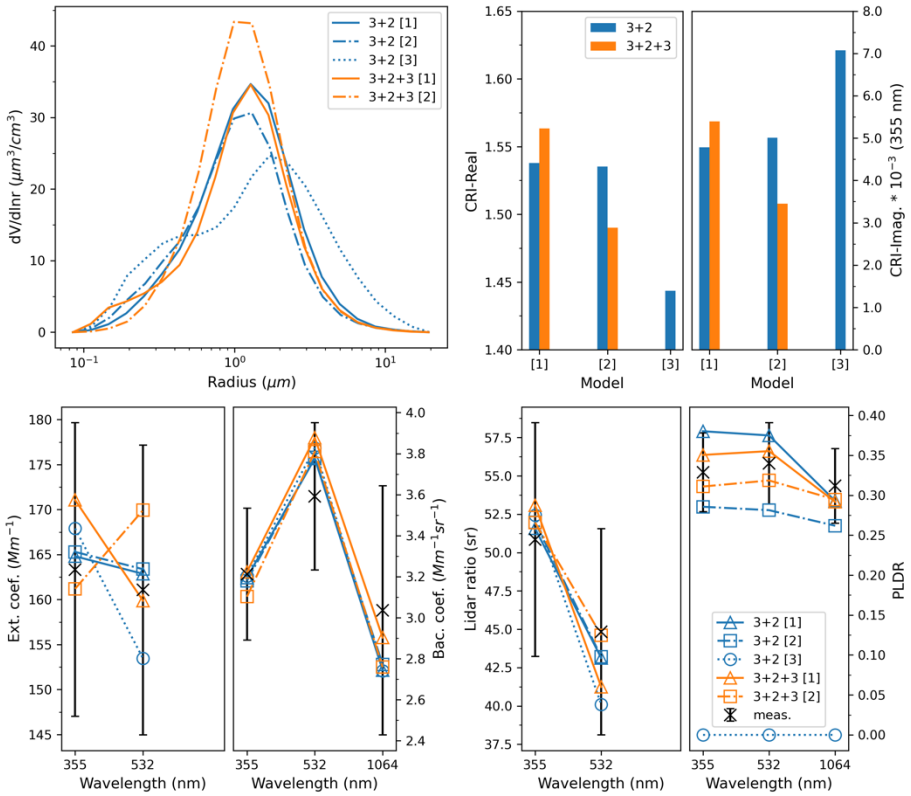

Figure 10. Retrieval of a real dust event measured by a Raman-polarization lidar on 15 April 2019 at Kashi, China. The period 17:00-22:00 UTC and layer 2-2.2 km are averaged (the optical profile can be found in Hu et al., 2020). The VSD, *n*, *k* and fitting to the measurements derived by using different scattering models ([1]: I-H, [2]: Spheroid, [3]: Sphere) and inverting different numbers of measurements are shown.

Reference:

Chang, Y., Hu, Q., Goloub, P., Veselovskii, I., and Podvin, T.: Retrieval of Aerosol Microphysical Properties from Multi-Wavelength Mie–Raman Lidar Using Maximum Likelihood Estimation: Algorithm, Performance, and Application, Remote Sensing, 14, 6208, https://doi.org/10.3390/rs14246208, 2022.

Dubovik, O., Sinyuk, A., Lapyonok, T., Holben, B. N., Mishchenko, M., Yang, P., Eck, T. F., Volten, H., Muñoz, O., Veihelmann, B., van der Zande, W. J., Leon, J.-F., Sorokin, M., and Slutsker, I.: Application of spheroid models to account for aerosol particle nonsphericity in remote sensing of desert dust, Journal of Geophysical Research: Atmospheres, 111, https://doi.org/10.1029/2005JD006619, 2006.

Hu, Q., Wang, H., Goloub, P., Li, Z., Veselovskii, I., Podvin, T., Li, K., and Korenskiy, M.: The characterization of Taklamakan dust properties using a multiwavelength Raman polarization lidar in Kashi, China, Atmospheric Chemistry and Physics, 20, 13817–13834, https://doi.org/10.5194/acp-20-13817-2020, 2020.

Saito, M., Yang, P., Ding, J., and Liu, X.: A Comprehensive Database of the Optical Properties of Irregular Aerosol Particles for Radiative Transfer Simulations, Journal of the Atmospheric Sciences, 78, 2089–2111, https://doi.org/10.1175/JAS-D-20-0338.1, 2021.